Monthly Notices
of the
ROYAL ASTRONOMICAL SOCIETY

MNRAS **454,** 1909–1920 (2015) doi:10.1093/mnras/stv2044

A SCUBA-2 850-μm survey of protoplanetary discs in the IC 348 cluster

L. Cieza,[1,2★] J. Williams,[3] E. Kourkchi,[3] S. Andrews,[4] S. Casassus,[2,5] S. Graves[6] and M. R. Schreiber[2,7]

[1]*Núcleo de Astronomía, Facultad de Ingeniería, Universidad Diego Portales, Av. Ejercito 441, Santiago, Chile*
[2]*Millenium Nucleus 'Protoplanetary discs in ALMA Early Science', Chile*
[3]*Institute for Astronomy, University of Hawaii at Manoa, Honolulu, HI 96822, USA*
[4]*Harvard–Smithsonian Center for Astrophysics, 60 Garden Street, Cambridge, MA 02138, USA*
[5]*Departamento de Astronomía, Universidad de Chile, Casilla 36-D Santiago, Chile*
[6]*Joint Astronomy Centre, 660 N. Aohoku Place, Hilo, HI 96720, USA*
[7]*Instituto de Astronomía y Astrofísica, Universidad de Valparaíso, Avda. Gran Bretaïa 1111, Valparaíso, Chile*

Accepted 2015 August 6. Received 2015 August 6; in original form 2015 April 24

ABSTRACT

We present 850-μm observations of the 2–3 Myr cluster IC 348 in the Perseus molecular cloud using the SCUBA-2 camera on the James Clerk Maxwell Telescope. Our SCUBA-2 map has a diameter of 30 arcmin and contains ∼370 cluster members, including ∼200 objects with IR excesses. We detect a total of 13 discs. Assuming standard dust properties and a gas-to-dust-mass ratio of 100, we derive disc masses ranging from 1.5 to 16 M_{JUP}. We also detect six Class 0/I protostars. We find that the most massive discs ($M_D > 3$ M_{JUP}; 850-μm flux > 10 mJy) in IC 348 tend to be transition objects according to the characteristic 'dip' in their infrared spectral energy distributions (SEDs). This trend is also seen in other regions. We speculate that this could be an initial conditions effect (e.g. more massive discs tend to form giant planets that result in transition disc SEDs) and/or a disc evolution effect (the formation of one or more massive planets results in both a transition disc SED and a reduction of the accretion rate, increasing the lifetime of the outer disc). A stacking analysis of the discs that remain undetected in our SCUBA-2 observations suggests that their median 850-μm flux should be $\lesssim$1 mJy, corresponding to a disc mass $\lesssim$0.3 M_{JUP} (gas plus dust) or $\lesssim$1 $M_\oplus$ of dust. While the available data are not deep enough to allow a meaningful comparison of the disc luminosity functions between IC 348 and other young stellar clusters, our results imply that disc masses exceeding the minimum-mass solar nebula are very rare ($\lesssim$1per cent) at the age of IC 348, especially around very low-mass stars.

Key words: protoplanetary discs – open clusters and associations: individual: IC 348 – submillimetre: planetary systems.

1 INTRODUCTION

Over the last decade, *Spitzer* has tremendously enriched our knowledge of the structure and evolution of circumstellar discs, the birth sites of planets. From *Spitzer* studies of molecular clouds and young stellar clusters, much has been learned about the infrared (IR) properties of pre-main-sequence (PMS) stars as a function of stellar age and mass (Carpenter et al. 2006; Allen et al. 2007; Hernández et al. 2007a,b; Kim et al. 2013). *Spitzer* observations have also revealed the diversity of radial structures that discs can present (e.g. holes and gaps) and the many evolutionary paths that discs can follow (Currie & Sicilia-Aguilar 2011; Williams & Cieza 2011; Espaillat et al. 2014).

While most protoplanetary discs remain optically thick in the IR, they become optically thin at longer wavelengths. Continuum (sub)millimeter observations are hence sensitive to dust properties (total dust masses and grain-size distributions) and are highly complementary to IR data. The (sub)millimeter luminosities of protoplanetary discs with almost identical IR spectral energy distributions (SEDs) can differ by up to two orders of magnitude (Cieza et al. 2008, 2010) implying drastically different disc masses and/or grain-size distributions; therefore, understanding disc evolution requires both IR and submillimeter observations.

Unfortunately, submillimeter surveys of discs in molecular clouds and young stellar clusters clearly lag behind their IR counterparts. While complete IR censuses of discs exist for tens of regions, there is only one region in which the entire disc population has been observed at (sub)millimeter wavelengths with enough depth to detect the majority of the IR-detected discs: the 1–2 Myr Taurus

★ E-mail: lucas.cieza@mail.udp.cl

molecular cloud (Andrews et al. 2013). In Taurus, the typical mass of a disc around a 1 $M_\odot$ star is ∼4 M_{JUP} and disc masses are roughly proportional to stellar mass (although there is a large dispersion for any given stellar mass). Our recent 850 μm SCUBA-2 observations of σ-Orionis (age ∼3–5 Myr; members ∼300) show that massive discs (>5 M_{JUP}) are rare (∼3per cent) around members of this older cluster (Williams et al. 2013). Even though those observations were insensitive to less-massive discs, a stacking analysis of the undetected sources suggests the mean mass of the IR-identified primordial discs ($N \sim 80$) is of the order of 0.5 M_{JUP}, indicating a rapid decline in the amount of raw material that is available for planet formation between the age of Taurus and the age of σ-Orionis.

Here, we present 850-μm SCUBA-2 observations of the IC 348 cluster, which is situated at the eastern edge of the Perseus molecular cloud complex, at a distance of 320 pc (Herbig 1998). IC 348 is a rich cluster partially embedded in natal gas and dust. This cluster has been extensively studied to determine its membership and contains >350 spectroscopically confirmed members (Luhman et al. 1998, 2003, 2005; Muench et al. 2007) with masses ranging from 0.02 to 5 $M_\odot$ and an estimated mean age of 2–3 Myr (Herbig 1998). This age range places IC 348 right in between Taurus and σ-Ori, which is consistent with its intermediate IR disc fraction of 50 per cent (Lada et al. 2006), to be compared with 63 per cent for Taurus (Hartmann et al. 2005) and 27 per cent for σ-Ori (Hernández et al. 2007a). IC 348 is slightly closer than σ-Orionis (320 versus 420 pc) and its 850-μm data is slightly deeper (2.7 mJy versus 2.9 mJy rms median noise). The resulting disc mass sensitivity is therefore a factor of ∼2.0 better in IC 348 than in σ-Ori (∼2.5 versus 5.0 M_{JUP})

IC 348 has already been observed at 1.3 mm with the Submillimeter Array (SMA; Lee, Williams & Cieza 2011). The 22 SMA fields from that study are each 55 arcsec in diameter and in total include 85 cluster members, about 25 per cent of the entire population. Nine young stellar objects were detected by the SMA with disc masses larger than ∼2 M_{JUP}. The 850-μm SCUBA-2 map presented here has a similar disc mass sensitivity, but covers all ∼370 cluster members. The SCUBA-2 observations are described in Section 2. The main results are shown in Section 3. In Section 4, we discuss the correlations between the (sub)millimeter and the IR properties of the targets and place our results in the general context of disc evolution and planet formation. Our main conclusions and a summary of the paper are presented in Section 5.

2 OBSERVATIONS

The IC 348 cluster was observed with SCUBA-2 using the 'pong-900' mapping mode resulting in a circular region with diameter of about 30 arcmin. The centre of the observed field is RA = $03^h44^m34^s$, DEC = $+32°07'48''$ and the observed area mostly covers the prominent star forming filaments of IC 348 at the north-east of the Perseus complex. The data were taken between 2011 October and 2013 October in queue mode over several observing runs (programme IDs: M11BH29B, M12AH29B, M12BH10C, and M13BH12A). The observations were performed under James Clerk Maxwell Telescope band-3 weather, which is defined based on the zenith optical depth at 225 GHz (τ_{225}) lying between 0.08 and 0.12. The actual τ_{225} value for each night is listed in Table 1. The total on-source integration time amounts to 22.4 h.

The pong-900 mapping mode provides fairly uniform sensitivity within a circular region of 20 arcmin in diameter. The useable area extends to a diameter of more than 25 arcmin in this mode, but with larger noise towards the edges. For data reduction, the Dynamic Iterative Map Maker in the STARLINK/SMURF software package (Chapin et al. 2013) was used at the Joint Astronomy Centre. Due to the existence of extended emission at 850 μm and because we were most interested in discs around stars, which would be point sources at the 15 arcsec SCUBA-2 resolution, we used the blank field configuration for the map maker which is usually used for deep field extragalactic surveys.

Table 1. Observing log.

Date	Programme ID	τ_{225}	T_{int} (h)
2011-10-24	M11BH29B	0.06	0.4
2011-10-25	M11BH29B	0.09	1.4
2011-11-10	M11BH29B	0.13	1.4
2011-12-17	M11BH29B	0.11	1.5
2012-02-03	M12AH29B	0.07	0.8
2012-08-24	M12BH10C	0.08	1.4
2012-08-25	M12BH10C	0.06	2.1
2012-08-26	M12BH10C	0.06	0.7
2012-08-27	M12BH10C	0.08	1.4
2013-01-07	M12BH10C	0.09	0.8
2013-09-21	M13BH12A	0.05	0.5
2013-09-23	M13BH12A	0.11	3.0
2013-09-24	M13BH12A	0.09	3.5
2013-10-29	M13BH12A	0.10	0.5
2013-10-30	M13BH12A	0.13	3.0
Total			22.4

The data were reduced night by night and then co-added with the weights proportional to the inverse square of the map noise. The flux density scale was estimated using the usual observations of the bright point sources, most commonly Uranus, Mars, and protoplanetary nebulae CRL 618 and CRL 2688. We reduced these sources with the same (blank field) map maker configuration file to derive the flux calibration factor (FCF). Following this procedure, we found FCF = 715 ± 70 Jy pW^{-1} $beam^{-1}$and therefore we multiplied the co-added map by this mean value.

At the end of the data processing, a matched beam filter was applied to smooth the data and maximize the sensitivity to point sources. Fig. 1 shows the final 850-μm map with 3 arcsec pixels we use for our study. Significant extended emission from the molecular cloud is seen towards the south and south-west of the map. SCUBA-2 observes at 850 and 450 μm simultaneously, but we do not use 450 μm data in our analysis because our programme does not meet the stringent weather requirements for sensitive 450 μm observations ($\tau_{225} < 0.05$).

3 RESULTS

3.1 Detections

We base our 850-μm analysis on the *Spitzer* sources studied by Lada et al. (2006, hereafter L06) and Muench et al. (2007, hereafter M07). Our SCUBA-2 map is ∼30 arcmin in diameter and contains the 307 cluster members studied by L06 and 62 of the 66 additional members studied by M07. As seen in Fig. 2, the L06 sources concentrate towards the centre of the map, while the M07 sources tend to lie towards the edges of the map and along the extended cloud emission seen in the south and south-west of the map. The L06 sources are confirmed cluster members from the spectroscopic study by Luhman et al. (2003), while the M07 sources are additional *Spitzer*-selected objects (i.e. objects with IR excesses).

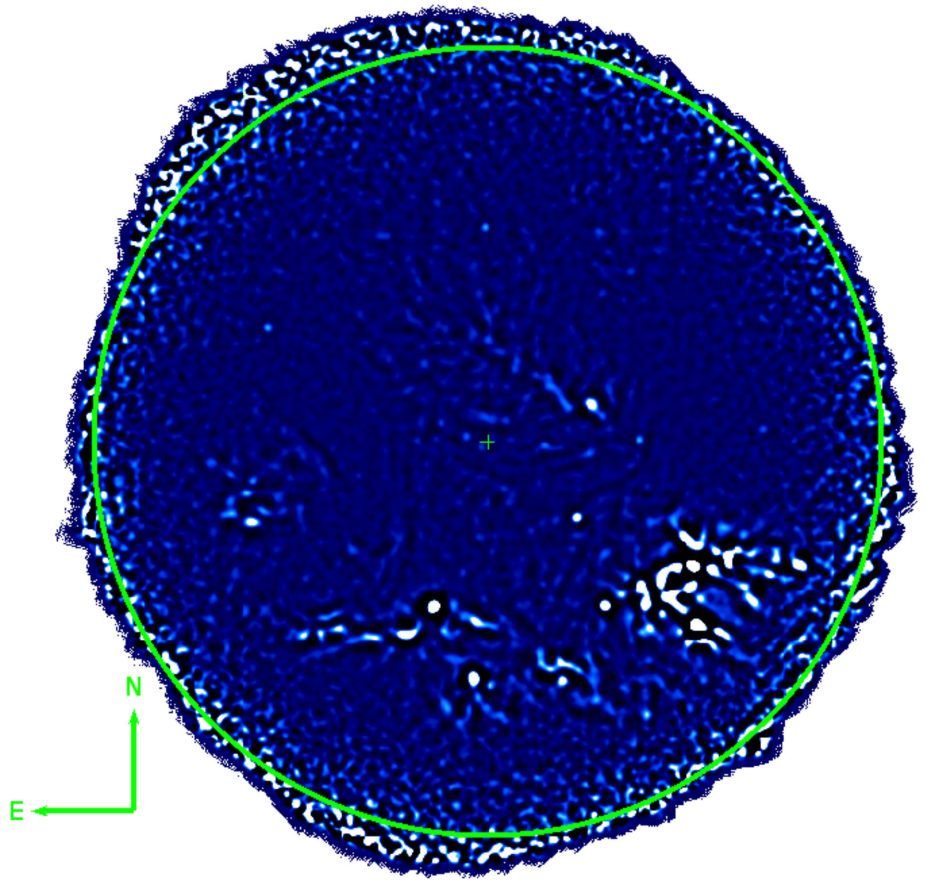

Figure 1. Our 850 μm SCUBA-2 map of the IC 348 cluster. The centre of the map is indicated by a '+' and corresponds to RA = $03^{h}04^{m}34^{s}$, Dec. = $+32°07'48''$s. As a scale reference, the green circle has a diameter of 30 arcmin. The noise is more or less uniform in the inner 25 arcmin region and degrades towards the edges. Significant extended emission from the molecular cloud can be seen in the south and south-west of the map.

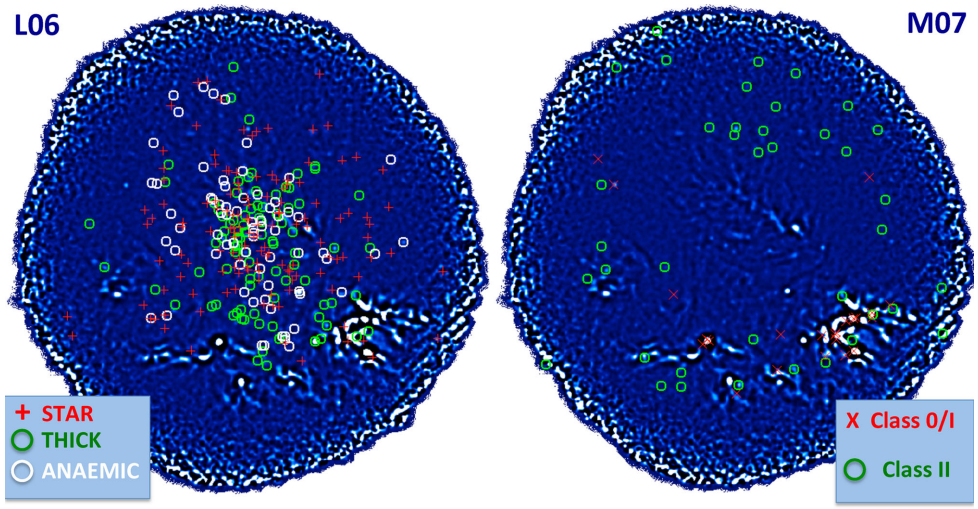

Figure 2. The spatial distributions of the different types of sources listed by L06 (left-hand panel) and M07 (right-hand panel). The sources from LO6 are distributed towards the centre of the map, while the sources from M07 tend to be located closer to the edges.

As a result, the latter group tend to be more embedded sources away from the centre of the SCUBA-2 map. This translates into higher noises in our 850-μm map. The median and mean noises of the L06 targets are 2.6 and 4.2 mJy, respectively, while the median and mean noises of the M07 sources are 5.5 and 24.7 mJy, respectively. Over the combined sample, L06 plus M07, the median and mean noises are 2.7 and 7.6 mJy, respectively. The large difference between the median and mean noises in the samples implies that the noise is far from homogenous across the map and strongly dependent on the underlying cloud emission.

Due to the variable background noise of our SCUBA-2 map, we adopt a very localized approach to perform our photometry and

Table 2. Detected discs (sorted by declining disc mass). (1) Source ID, coordinates, spectral types and H α EWs from Luhman et al. (2003) or M07. (2) Object type from L06 or M07 this paper. (3) 850-μm flux from our SCUBA-2 data. (4) 860-μm flux from SMA data (Espaillat et al. 2012). (5) 1300-μm flux from SMA (Lee et al. 2011). (6) disc mass derived as described in Section 4.1 for SCUBA-2 detections, or taken from Lee et al. (2011) for objects detected only at 1300 μm.

ID	RA (J2000) (°)	Dec. (J2000) (°)	SpT	Disc Class	F_{850} (mJy)	F_{860} (mJy)	F_{1300} (mJy)	EW$_{H\alpha}$ (Å)	$M_{\rm disc}$ ($M_{\rm JUP}$)
(1)	(1)	(1)	(1)	(2)	(3)	(4)	(5)	(1)	(6)
31	56.075 83	32.082 50	G1	ANEMIC/TD	52.9 ± 4.0	62 ± 6.0	–	11 ± 0.5	16.0
329	56.064 90	32.156 09	M7.5	STAR/TD	42.0 ± 11	–	–	–	12.6
156	56.028 33	32.131 72	M4	THICK/II	21.2 ± 1.7	–	–	10.0 ± 2	6.4
265	56.144 58	32.266 66	M3.5	II/TD	21.1 ± 1.6	–	–	–	6.4
1933	56.318 12	32.105 53	K5	II	15.2 ± 5.0	–	–	–	4.6
32	56.157 92	32.134 50	K7	THICK/TD	14.2 ± 2.0	–	5.50 ± 0.80	68 ± 1	4.3
10 352	56.335 25	32.109 56	M1	THICK/II	13.2 ± 2.9	–	11.5 ± 1.0	–	4.0
67	55.935 83	32.138 31	M0	ANEMIC/TD	12.1 ± 1.7	25 ± 11	–	35 ± 2	3.6
221	56.167 72	32.159 23	M4.5	THICK/II	–	–	3.23 ± 0.89	40 ± 5	2.9
9024	56.147 39	32.126 71	M0	THICK/II	9.3 ± 1.5	–	–	–	2.8
153	56.178 22	32.142 73	M4.75	THICK/II	9.2 ± 2.8	–	6.49 ± 0.71	40 ± 10	2.8
248	56.149 78	32.156 74	M5.25	THICK/II	–	–	2.81 ± 0.81	30 ± 5	2.6
468	56.046 13	32.028 80	M8.25	THICK/II	–	–	2.37 ± 0.56	400 ± 50	2.2
5	56.108 44	32.075 11	G8	THICK/II	6.3 ± 1.8	–	–	–	1.9
8078	56.111 20	32.138 97	M0.5	THICK/II	–	–	2.07 ± 0.51	75	1.9
100	56.093 01	32.200 21	M1	THICK/II	–	–	2.06 ± 0.51	90	1.9
192	56.098 50	32.031 30	M4.5	THICK/II	–	–	2.06 ± 0.57	40 ± 20	1.9
19	56.128 42	32.165 50	A2	THICK/II	5.9 ± 1.7	–	–	–	1.8
15	56.186 31	32.067 42	M0.5	THICK/II	–	–	1.98 ± 0.46	36	1.8
117	55.996 17	32.239 25	M3	II	5.1 ± 1.3	–	–	–	1.5

derive the fluxes from a single pixel (3 arcsec on a side and in units of mJy beam^{-1}), corresponding to the nominal location of the sources (based on their *Spitzer* coordinates). In the context of point spread function (PSF)-fitting photometry, this is analogous to scaling a PSF to the central pixel, instead of allowing for a small error in position and fitting the entire PSF, which would increase the chances of confusing a local peak in the background with a real source. To estimate the background noise, we use a rather small annulus with an inner and outer radius of 15 and 30 arcsec, respectively (to obtain a localized measurement of the noise).

Using this approach, we detect 21 members with signal-to-noise ratios >3.0. 13 of these members were classified by L06 and M07 as circumstellar discs (anemic, thick, and Class II in their nomenclature) based on their near-IR properties, while the other six objects are protostars (Class 0/I sources), where the 850-μm flux is likely to be dominated by their envelopes as opposed to their discs. The properties of the 13 discs are listed in Table 2 and their locations are shown in Fig. 3 (left-hand panel). For identification purposes, we adopt the ID numbers used by Luhman et al. 2003, L06, and M07. Close-up images of the 13 detected discs are shown in Fig. 4.

Four out of the 13 discs detected at 850-μm, sources no. 19, 32, 51, and 153, fall within the SMA fields observed at 1.3 mm by Lee at al. (2011), see Fig. 3. All of them were detected by the SMA, except for no. 19, the faintest of the four. This object is 5.9 ± 1.7 mJy and thus only marginally detected (3.5σ) at 850 μm; however, its SCUBA-2 detection is still consistent with the SMA non-detection, given the noise of the 1.3 mm observations (3σ = 2.2 mJy) and the observed 850 μm to 1.3 mm flux ratios of other objects in the sample (e.g. 2.6 for source no. 32). Lee et al. (2011) also detected seven objects that were not detected in our SCUBA-2 map. Their 1.3 mm fluxes are in the ∼2–3 mJy range and their SCUBA-2 non-detections are also consistent with the 850-μm noise levels at their location (∼2–3 mJy). These seven objects are also listed in Table 2.

In this study, we focus on the disc sources in IC 348. For completeness, we note that we also detected 6 of the 23 Class 0/I objects listed by M07 (see Table 3). Their fluxes range from ∼450 to 750 mJy for Class 0 sources and ∼20 to 200 mJy for Class I objects. Their locations are shown in Fig. 3 (right-hand panel) and their close-up images in Fig. 5. Most of the protostars identified by M07 are located in the regions of strongest cloud emission, which is likely to account for our non-detections. However, we note that four of these undetected Class 0/I objects (objects no. 21799, 22903, 1401, and 52590 in M07) are in regions free of cloud contamination and are likely to be background galaxies, as already suggested by M07.

3.2 Stacking of non-detections

Even though its IR disc fraction is close to 50 per cent, the vast majority of the cluster members in IC 348 remain undetected at 850 μm. Still, it is possible to place some constraints on the typical submillimeter properties of the undetected discs from the statistics of the measured SCUBA-2 fluxes at the locations of the targets (i.e. by stacking the non-detections). L06 classified the discs in IC 348 based on the slope of the SED at IRAC[1] wavelengths (3.6–8.0 μm), $\alpha_{\rm IRAC} = {\rm d}\log\lambda F_\lambda / {\rm d}\log\lambda$, from a power-law, least-squares fit to the four IRAC bands for each star. In particular, objects with $\alpha_{\rm IRAC} > -1.8$ were classified as optically thick discs, while objects with $-2.56 < \alpha_{\rm IRAC} < -1.8$ were dubbed 'anemic' discs. Objects with $\alpha_{\rm IRAC} < -2.56$ were regarded as discless. This classification is mostly empirical and is based on the fact that the $\alpha_{\rm IRAC}$ values of PMS stars in Taurus are well separated in two groups, those with $\alpha_{\rm IRAC} < -2.56$, in agreement with the predicted slope for an M0 star, and those with $\alpha_{\rm IRAC} > -1.8$, in agreement with the predictions

[1] *Spitzer*'s IR Array Camera.

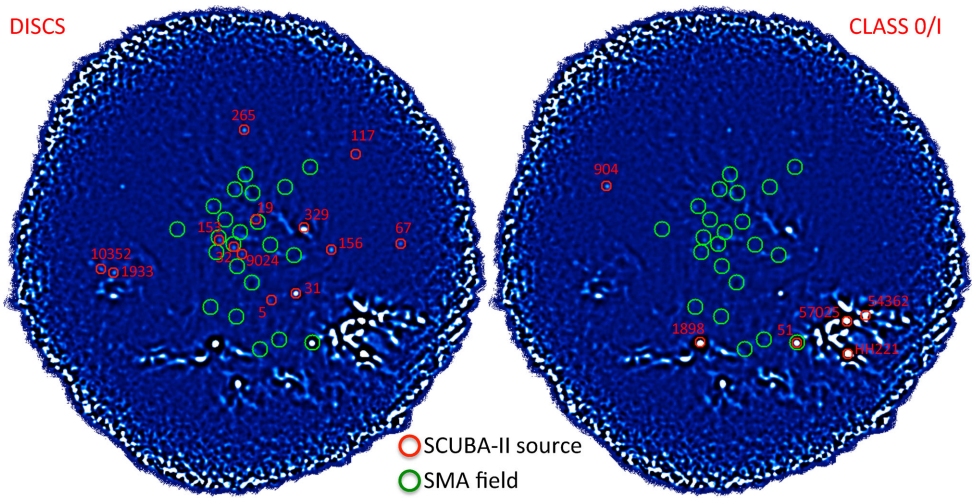

Figure 3. The locations of our SCUBA-2 detections. The discs (anemic, thick and Class-II sources) are shown in the left-hand panel. Class 0/I protostars are shown in the right-hand panel. Four of our SCUBA-2 sources, no. 19, 32, 51, and 153, fall in the SMA fields observed by Lee et al. (2011), shown as green circles, 55 arcsec in diameter.

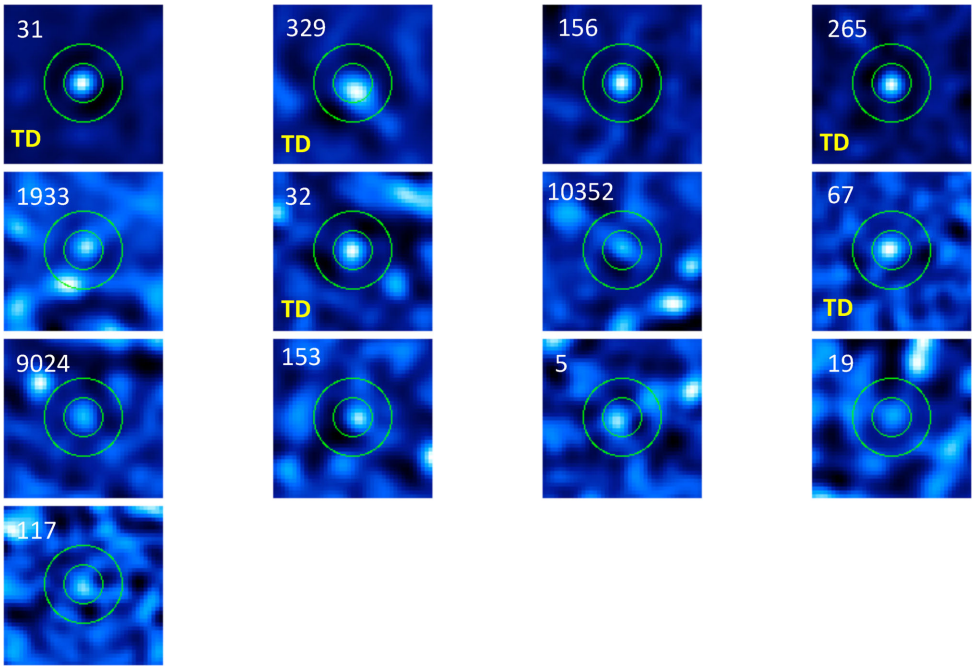

Figure 4. The 13 discs detected in our SCUBA-2 map ordered by decreasing 850 μm flux. Five objects with transition disc SEDs are labelled 'TD' and are among the brightest eight sources. The green circles are 15 and 30 arcsec in radius. The annuli within the circles are used to estimate the local noise of the map around each source.

for optically thick discs extending inwards to the dust sublimation radius. Objects with intermediate $\alpha_{\rm IRAC}$ values were later seen in IC 348. They were interpreted as heavily depleted or optically thin discs and grouped in the intermediate 'anemic' disc category. Similarly, M07 classified the sources with $-0.5 > \alpha_{\rm IRAC} > -1.8$ as Class II and sources with $\alpha_{\rm IRAC} > -0.5$ as Class 0/I protostars. M07 does not report objects with weak excesses (anemic discs). For our stacking analysis, we adopt the disc classification from L06 and M07 as a simple metric to characterize the strength of the IR disc emission, but note some caveats. First, the $\alpha_{\rm IRAC}$ classification is based on short IR wavelengths (<10 μm) and could misrepresent objects with large inner holes that are characterized by weak IR excesses at $\lambda < 10\,\mu$m, but strong excesses at longer IR wavelengths (i.e. transition discs). Also, the stellar photospheres of the lowest mass members of the cluster are faint at 8.0 μm and their photometry is quite noisy. As a result, the significance of the IR excesses of many of the anemic discs listed by L06 is low ($<3\sigma$) and some of the objects might be in fact discless stars (Cieza et al. 2007; M07). However, these caveats should only have a minor effect on the overall statistics.

For the stacking analysis, we produce average and median images of all subsamples (discless stars, anemic discs, and thick discs from L06 and Class-II discs from M07) and some combinations of subsamples (thick discs plus anemic discs from L06 and thick discs from L06 plus Class-II objects from M07). Before stacking, we remove all sources that are individually detected and also mask

Table 3. Detected protostars (sorted by declining flux). (1) Source ID, coordinates, and object type from Luhman et al. (2003) or M07.

ID	Ra (J2000) (°)	Dec (J2000) (°)	Object Class	F_{850} (mJy)
(1)	(1)	(1)	(1)	
57025	55.987 04	32.050 94	0	756 ± 85
HH221	55.986 54	32.013 86	0	727 ± 98
1898	56.182 88	32.027 04	0/I	451 ± 23
54362	55.962 28	32.057 29	I	189 ± 33
51	56.054 17	32.026 50	I	129 ± 10
904	56.307 54	32.202 81	I	19 ± 1.4

all pixels with values larger than 10 mJy or smaller than –10 mJy in the individual images to eliminate particularly noisy regions of the mosaic. The resulting images are shown in Fig. 6. We then perform the photometry as described in the previous section. As shown in Table 4 and Fig. 6, only the stacking of the thick discs and the thick discs plus the Class-II sources result in possible detections at the 2.7σ–3.5σ level and a flux of ∼0.7–1.0 mJy. We regard these detections as tentative and conclude that the discs that are optically thick in the IR but remain individually undetected in our SCUBA-2 map have a median 850-μm flux $\lesssim$1.0 mJy.

4 DISCUSSION

4.1 Disc masses

Since discs become optically thin at submillimeter wavelengths, all dust grains contribute to the emission and the total flux correlates well with the total dust mass. (Sub)millimeter fluxes are thus routinely used to estimate the masses of protoplanetary discs using the following formula:

$$M_{\rm dust} = \frac{F_\nu\, d^2}{\kappa_\nu\, B_\nu\, (T_{\rm dust})}, \quad (1)$$

where d is the distance to the target, T is the dust temperature and κ_ν is the dust opacity. Adopting a distance of 320 pc, and by making standard (although uncertain) assumptions about the disc temperature ($T_{\rm dust} = 20$ K) and dust opacity ($\kappa_\nu = 10(\nu/1200\,{\rm GHz})\,{\rm cm^2\,g^{-1}}$, following Beckwith et al. (1990), equation (1) becomes

$$M_{\rm dust}[{\rm M}_\oplus] = 0.97 \times F_{850}\,({\rm mJy}). \quad (2)$$

From equation (2) and adopting a gas-to-dust-mass ratio of 100 (the canonical value used for the interstellar medium), the total disc mass can be estimated as follows:

$$M_{\rm disc}[M_{\rm JUP}] = 0.30 \times F_{850}\,({\rm mJy}). \quad (3)$$

The disc masses so calculated for our SCUBA-2 detections are listed in Table 2. The disc masses for the seven objects that were only detected by the SMA at 1.3 mm were taken directly from Lee et al. (2011), but were calculated using the same approach. The uncertainties in the dust opacity and gas-to-dust-mass ratio are significant, but the adopted values are quite standard in the literature, allowing for meaningful comparisons to other studies. The detected disc have modest masses, ranging from 1.5 to 16 $M_{\rm JUP}$. The median noise of the IC 348 cluster members is 2.7 mJy, which translates to a 3σ disc mass of 2.4 $M_{\rm JUP}$; therefore, our survey can be considered to be complete down to this level in regions free of contamination from cloud emission.

4.2 Non-detections

Equations (2) and (3) can also be used to place upper limits to the typical dust and disc masses of the undetected discs in IC 348. The ∼1.0 mJy marginal detections in the stacking analysis of the 'thick' and Class-II discs translate to dust mass of $\lesssim$1.0 $M_\oplus$, corresponding to a disc mass of $\lesssim$ 0.3 $M_{\rm JUP}$ assuming a gas-to-dust-mass ratio of 100. Williams et al. (2013) performed a similar stacking analysis for the SCUBA-2 non-detections towards IR-detected discs in the σ-Orionis cluster and found a positive signal (3.3σ significance), consistent with an average disc mass of 0.54 $M_{\rm JUP}$. Since σ-Orionis is an older region than IC 348, we speculate that the lower mass of the average disc in IC 348 is a host mass effect: there is a higher incidence of very low mass stars (late M-type) in IC 348 and disc

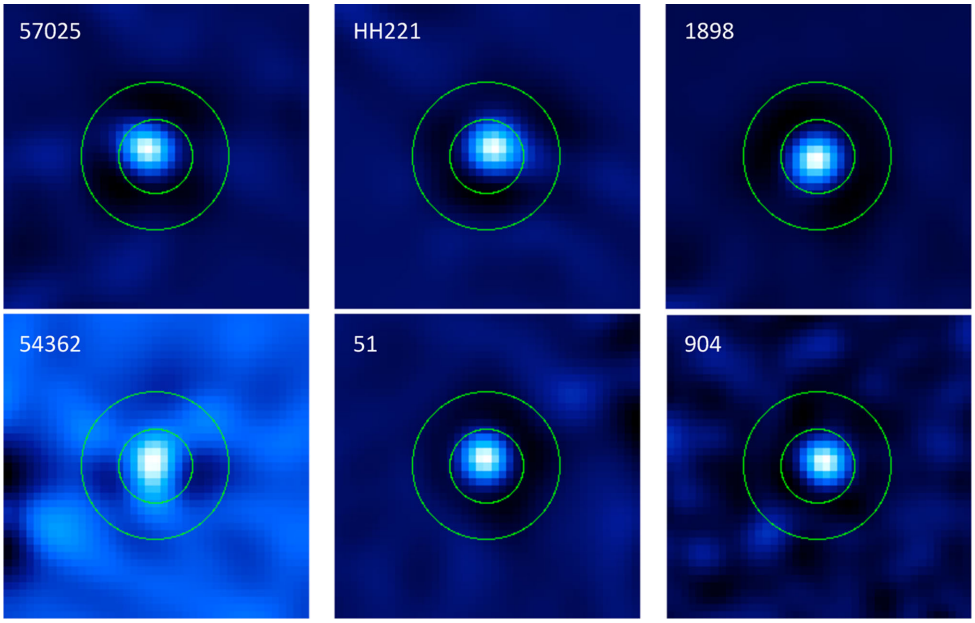

Figure 5. The six protostars detected in our SCUBA-2 map ordered by decreasing 850-μm flux. The green circles are 15 and 30 arcsec in radius. The annuli within the circles are used to estimate the local noise of the map around each source.

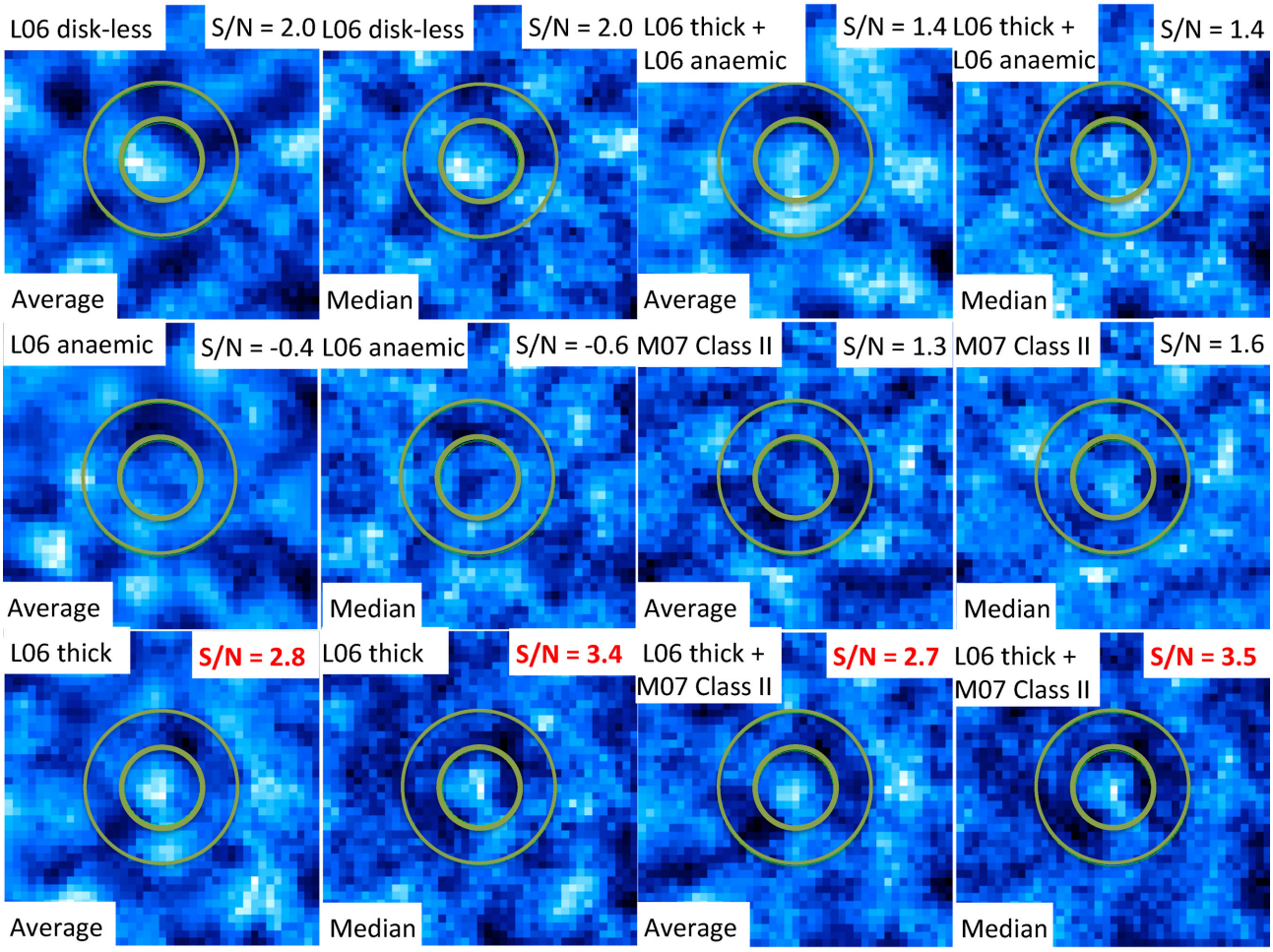

Figure 6. Stacked images (average and median) for all subsamples (discless stars, anemic discs, and thick discs from L06 and Class-II discs from M07) and some combinations of subsamples (thick discs plus anemic discs from L06 and thick discs from L06 plus Class-II objects from M07). The images are 1 arcmin on the side. Only the stacking of the thick discs and the thick discs plus Class-II sources show tentative detections at the 2.7σ–3.5σ level (bottom rows).

Table 4. Stacking photometry.

Sample	Sample size	Average (mJy)	Median (mJy)
L06 discless	134	0.46 ± 0.23	0.50 ± 0.25
L06 anemic	67	-0.12 ± 0.28	-0.19 ± 0.30
L06 thick	**83**	$\mathbf{0.79 \pm 0.28}$	$\mathbf{1.01 \pm 0.30}$
L06 thick + anemic	150	0.30 ± 0.22	0.35 ± 0.25
M07 Class II	35	0.78 ± 0.59	0.95 ± 0.61
M07 Class II + L06 thick	**118**	$\mathbf{0.69 \pm 0.26}$	$\mathbf{1.02 \pm 0.29}$

masses are known to scale with the mass of the central star (Andrews et al. 2013).

4.3 Correlation between submm and IR properties

In order to investigate a possible correlation between the submillimeter and the IR properties of the discs in IC 348, we first construct their SEDs, using the photometry listed in Table 5. For consistency, we adopt the IR fluxes (1.25–70 μm) from the catalogues of the *Spitzer* Legacy Programme 'From Molecular Cores to Planet-forming discs' (Evans et al. 2009; Wright et al. 2010). We also collect available optical photometry from the literature (Luhman et al. 2003; Littlefair et al. 2005; Cieza & Baliber 2006; Cieza et al. 2007). We correct the optical and near-IR fluxes for extinction, adopting $A_V = 5.88 \times [(J-K)-(J-K)_0]$, where $(J-K)_0$ is the intrinsic colour of the star of a given spectral type, which is taken from Kenyon & Hartmann (1995). When available in the *Spitzer* archive,[2] we also collected the spectra of *Spitzer*'s IR Spectrograph (IRS).

The resulting SEDs for the 13 discs detected by our SCUBA-2 observations are shown in Fig. 7 ordered by decreasing 850 μm flux. One object, no. 329 has no 24 μm detection in the *Spitzer* catalogues. Instead, we plot their 12 and 22 μm fluxes from the *Wide field IR Survey Explorer* (*WISE*) catalogue[3] (9.52 ± 0.16 and 7.35 ± 0.16 mag, respectively). We find that five of the eight discs that are brightest at 850 μm (sources no. 31, 329, 265, 32, and 67, $M_D > 3.0\,M_{JUP}$) have the mid-IR 'dip' that indicates the presence of an inner hole or a gap, which are the defining features of transitions discs. The SEDs of the seven sources that were detected by the SMA at 1.3 mm (Lee et al. 2011) but remained undetected in our SCUBA-2 maps are not shown here, but they all have 'normal' SEDs close to the median of Classical T Tauri stars (see their fig. 4). They also

[2] http://archive.spitzer.caltech.edu/
[3] http://irsa.ipac.caltech.edu/Missions/wise.html

Table 5. Optical and IR photometry for detected discs (sorted by declining disc mass).

ID	*R* band (mag)	*I* band (mag)	*J* band (mJy)	*H* band (mJy)	*K* band (mJy)	$F_{3.6}$ (mJy)	$F_{4.5}$ (mJy)	$F_{5.8}$ (mJy)	$F_{8.0}$ (mJy)	F_{24} (mJy)	F_{70} (mJy)
31	–	15.37	23.20	62.20	88.80	75.59	54.10	66.20	53.40	469.00	–
329	20.17	17.64	2.32	3.16	3.19	2.04	1.55	1.11	0.65	–.	–
156	17.27	15.48	9.83	14.20	13.30	10.90	9.35	8.46	9.30	14.30	–
265	–	–	0.88	4.58	10.60	11.80	13.80	13.60	15.90	125.00	–
1933	–	–	25.00	62.00	97.30	140.00	183.00	180.00	252.00	373.00	445
32	–	14.18	33.70	65.90	77.90	69.10	69.60	54.10	67.00	89.40	–
10 352	14.90	13.42	57.00	104.00	122.00	92.10	88.50	74.20	83.10	204.00	357
67	–	13.93	24.10	36.09	32.09	19.00	14.90	11.40	10.90	104.00	173
9024	–	–	23.50	43.00	46.40	28.30	29.50	25.30	37.30	48.70	–
153	–	15.95	8.18	13.30	13.80	11.40	9.84	10.30	10.50	13.60	–
5	13.79	12.44	149.00	291.00	371.00	389.00	375.00	349.00	369.00	474.00	–
19	–	10.81	186.00	151.00	112.00	51.20	35.29	41.20	74.09	25.80	–
117	17.27	15.82	6.42	12.50	18.60	13.30	14.60	12.00	13.70	23.30	–

Notes. Optical Photometry comes from Luhman et al. (2003), Littlefair et al. (2005), Cieza & Baliber (2006) and Cieza et al. (2007) comes from *Spitzer's Cores to Discs* catalogue (Evans et al. 2009).

have lower disc masses than any of the transition discs in our sample ($M_D < 3\ M_{JUP}$).

The correlation between a large 850-μm flux and a transition disc SED seems to be robust. We note that three of these five transition discs (sources no. 31, 32, and 67) have already been detected with the SMA (Lee et al. 2011, Espaillat et al. 2012) and that object no. 265 has a very secure SCUBA-2 detection (S/N ∼14). Source no. 329 is bright, but slightly elongated towards the south-west. Still, we find no other 2MASS, *WISE*, or *Spitzer* object within 20 arcsec of this source and consider the 850-μm detection to be associated with this object, although cloud contamination cannot be ruled out.

To establish how statistically significant this correlation is, we first need to estimate the number of transition discs present in IC 348. This is a non-trivial task as no standard definition exists for transition objects and their identification also depends on the available data. For instance, object no. 32 can be identified as a transition disc based on the IRS spectra, but its broad-band photometry seems rather 'normal'. To address this problem, we plot the [8.0–24] versus [3.6–4.5] colour–colour diagram (see Fig. 8) for our entire sample of discs (thick, anemic, and Class-II sources). Transition discs can be characterized by a steeply rising mid-IR SED (e.g. Espaillat et al. 2012). The [8.0–24] colour nicely captures this feature, except for objects with very large inner holes. In fact, all transition discs in our SCUBA-2 sample have [8.0–24] > 4.4, except for object no. 32. From Fig. 8, we conclude that 66.7 per cent (4/6) of the objects with [8.0–24] > 4.4 have massive discs ($M_D > 3\ M_{JUP}$), while only 3 per cent (4/127) of the objects with [8.0–24] < 4.4 do so. To further quantify the significance of this correlation, we perform a Kolmogorov–Smirnov test to estimate the probability that the [8.0–24] colours of the discs with masses smaller and larger than $3\ M_{JUP}$ are drawn from the same parent population. We find that the Kolmogorov–Smirnov statistic, *d* (the maximum deviation between the cumulative distributions), is 0.48, and that the probability of the two distributions been drawn from the same parent population is 3 per cent. The modest significance of the test for the given *d* number is due to the small size of the transition disc sample.

A similar connection between massive discs and transition disc SEDs is found in other regions. For instance, in σ-Ori, Williams et al. (2013) also noted that three out of the eight discs detected at 850 μm are transition objects. Furthermore, the most massive discs in older regions such as Upper Scorpius and the TW Hydra Association are also transition objects: [PZ99] J160421.7-213028 (Mathews, Williams & Ménard 2012) and TW Hydra itself (Calvet et al. 2002).

The origin of transition discs is still a matter of intense debate (see Espaillat et al. 2014 for a recent review), and several mechanisms have been proposed to explain their inner holes, including grain growth (Dullemond & Dominik 2005), photoevaporation (Gorti & Hollenbach 2009), and the dynamical interaction with (sub)stellar objects (Quillen et al. 2004). However, grain growth alone has been shown to be an inefficient hole formation mechanism as dust fragmentation and radial drift result in the efficient replenishment of micron-size grains (Brauer, Dullemond & Henning 2008; Birnstiel, Andrews & Ercolano 2012). Also, while a few transition discs such as CoKu Tau/4 were found to be close stellar binaries (Ireland & Kraus 2008) and massive circumbinary discs do exist (e.g. GG Tau; Guilloteau, Dutrey & Simon 1999), it soon became clear that most transition discs are not due to binarity (Pott et al. 2010). There seem to be distinct populations of transition objects (Owen & Clarke 2012), and massive discs with large inner holes are believed to be carved by recently formed massive planets (Najita, Strom & Muzerolle 2007; Cieza et al. 2012a,b; Kraus & Ireland 2012; Kim et al. 2013).

In this context, we speculate that the correlation between a large disc mass and a transition disc SED could be an initial conditions effect. Recent statistics on extrasolar planets imply that the usual outcome of disc evolution is a planetary system (Howard et al. 2010). However, massive planets are relatively rare (Fressin et al. 2013) and not all discs will form planets massive enough to open wide gaps in the disc (Dodson-Robinson & Salyk 2011; Zhu et al. 2011). More massive discs will naturally tend to form more massive planets (Mordasini et al. 2012), which in turn will result in transition disc SEDs. We also note that disc evolution coupled to planet formation *could* also re-enforce this trend. Najita et al. (2007) showed that transition discs tend to have stellar accretion rates ∼10 times lower and median disc masses ∼4 times larger than non-transition objects. Massive enough planets could reduce or stop accretion on to the star by isolating the inner and outer discs (Lubow, Seibert & Artymowicz 1999); therefore, the formation of one or more massive planets could result in both a transition disc SED and a reduction in the accretion rate, increasing the lifetime of the outer disc. However, the formation of a gap by a massive planet may also have the opposite effect on the lifetime of the outer disc as the inner edge of the gap could be directly exposed to stellar radiation and photoevaporate

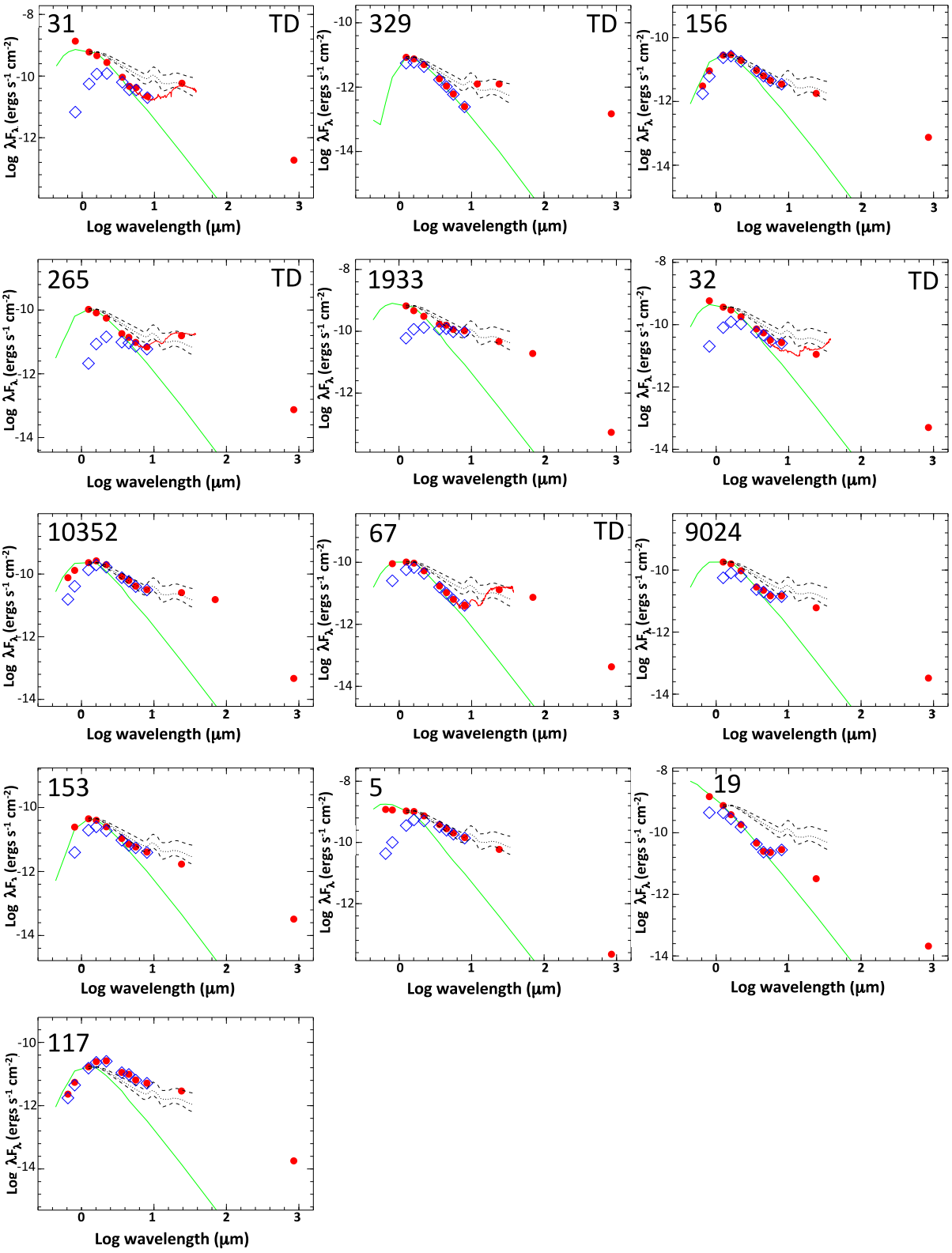

Figure 7. The SEDs of the 13 discs detected in our SCUBA-2 map ordered by decreasing 850-μm flux. Five objects with transition disc SEDs are labelled 'TD' and are among the brightest eight sources. The green lines are the stellar photospheres. The blue boxes represent the observed optical and IR photometry before correcting for extinction. The dotted lines correspond to the median mid-IR SED of K5–M2 CTTSs calculated by Furlan et al. (2006). The dashed lines are the quartiles.

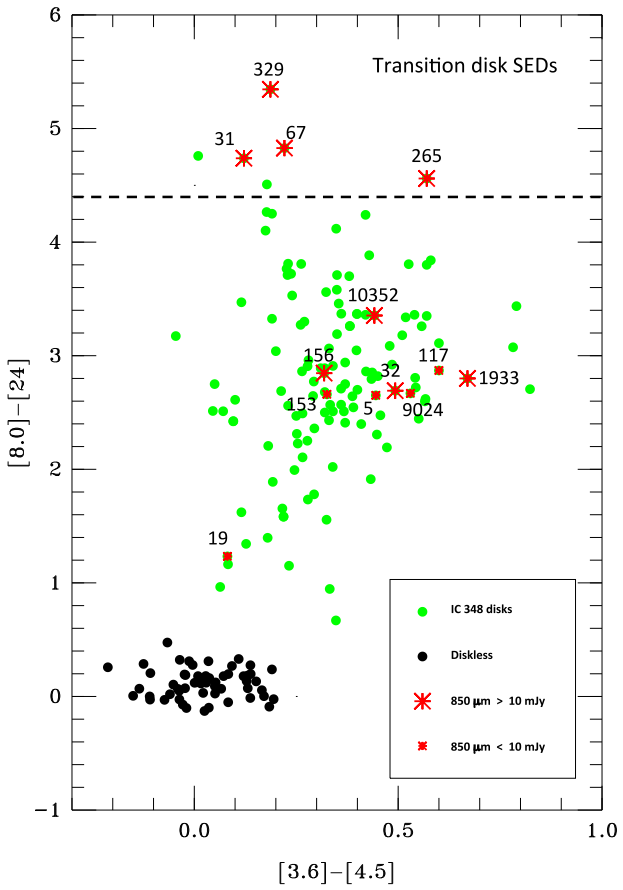

Figure 8. The *Spitzer* [8.0–24] versus [3.6–4.5] colour-colour diagram for discs in IC 348 (thick and anemic discs from L06 and Class-II objects from M07). Our 850-μm detections are individually labelled. Discless weak-line T Tauri stars from Cieza et al. (2007) are shown to illustrate the locus of bare stellar photospheres. Transition objects have very red [8.0–24] colours as their SEDs that are steeply rising in the mid-IR, indicating the presence of inner holes in their discs. There is a clear correlation in our sample between a transition disc SED and a bright 850-μm flux. Four out of the six discs with the reddest [8.0–24] colours are among the brightest SCUBA-2 detections (850-μm flux > 10 mJy).

more efficiently (Owen, Ercolano & Clarke 2011). The net result of the formation of a gap by a massive planet (an increase versus a decrease in the lifetime of the outer disc) will depend on whether photoevaporation rates can approach the accretion rates of T Tauri stars, which is also still a matter of intense debate (see Alexander et al. 2014 for a recent review).

4.4 Comparison to other regions

Investigating the evolution of disc masses as a function of stellar age is of critical importance to planet formation theory as it provides a first-coder approximation of the amount of raw material still available for planet building. However, comparing disc mass distributions between regions of different ages is complicated by low detection rates at millimeter wavelengths (Williams et al. 2013; Dodds et al. 2015) and the strong dependence of the millimeter wavelength luminosity on stellar mass ($L_{\rm mm} \propto {\rm M}^{1.5-2.0}$; Andrews et al. 2013). To take into account the host mass effect, we follow the methodology introduced in Andrews et al. (2013) to compare the disc masses in IC 348 with those in Taurus. Taurus is a well-studied region for which we have the disc mass distribution for each spectral type. Nevertheless, even in Taurus the millimeter detection rate is a strong function of spectral type: it is close to 100 per cent for stars K6 and earlier, but drops to $\lesssim$30 per cent for M3.5- to M6-type stars.

Based on the spectral type of the host stars in IC 348, we can associate their stellar mass to the disc properties observed in Taurus. Thus, using the spectral type of all IC 348 discs, we can generate many sets of random ensembles based on Taurus disc luminosity distributions (see Fig. 9, left-hand panel). For this study, we simulate 10^5 synthetic Taurus disc ensembles that resemble to IC 348 in terms of their stellar spectral types (i.e. dominated by M3- to M6-type stars). Then, using the two-sample test for censored data sets (Feigelson & Nelson 1985), we compare the actual SCUBA-2 observations with the simulated Taurus ensembles to find the probability that they are not originated from the same parent distribution, p_ϕ. The cumulative probability distribution, f ($<p_\phi$), is presented in Fig. 9 and indicates that there is a 5 per cent chance that the 850-μm disc luminosity distribution in IC 348 is different from Taurus at $>2\sigma$ significance. For comparison, we plot the results of the same analysis for the ρ Ophiuchus star-forming region and Upper Scorpius from Andrews et al. (2013) and σ-Orionis from Williams et al. (2013).

Given the available data, only the disc luminosity distribution of σ-Orionis (age ∼3–5 Myr, IR disc fraction ∼27 per cent; Williams et al. 2013) is significant different ($>3\sigma$) from that of Taurus (age ∼1–3 Myr, IR disc fraction ∼67 per cent; Rebull et al. 2010); nevertheless, we emphasize that these statistical tests are based on very incomplete data sets and should be interpreted with caution. PMS star ages are very uncertain, but IC 348 has an IR disc fraction of ∼50 per cent and an estimated age of 2–3 Myr (L06), and thus is particularly useful to establish the distribution of disc masses at the time half the disc population has already dissipated. However, we conclude that much deeper millimeter wavelength surveys are needed to investigate disc mass distributions as a function of cluster age in detail.

On the other hand, current millimeter surveys do provide valuable information on the incidence of very massive discs in young stellar cluster. As discussed by Dodds et al. (2015), discs exceeding the canonical minimum-mass solar nebula (MMSN), ranging from 10 to 100 Jupiter masses (Weidenschilling 1977), are relative rare ($\lesssim$10–20 per cent) in young clusters. Our results in IC 348 strengthen this conclusion since only 2 out of 370 (∼0.5 per cent) cluster members in our SCUBA-2 field (objects no. 31 and 329) have disc masses larger than 10 $M_{\rm JUP}$. The fact that massive discs are rare, *especially* around very low-mass stars, is in agreement with both the lower incidence of giant planets compared to terrestrial planets (Ford 2014) and the lower fraction of M-type stars hosting Jovian planets with respect to solar-type stars (Clanton & Gaudi 2014).

5 CONCLUSIONS

We have observed ∼370 members of the 2–3 Myr cluster IC 348. We have detected a total of 13 discs, raising the total number of detections in the cluster to 20. We have also detected six Class 0/I protostars. The detected discs have inferred masses ranging from 1.5 to 16 $M_{\rm JUP}$. Our results imply that disc masses exceeding the MMSN are very rare ($\lesssim$1 per cent) at the age of IC 348, specially around very low-mass stars. In our sample, we find a strong correlation between a relatively massive disc ($M_{\rm D} > 3\ M_{\rm JUP}$) and a transition disc SED. Pending confirmation that these transition systems are *not* circumbinary discs, we suggest that this could be an

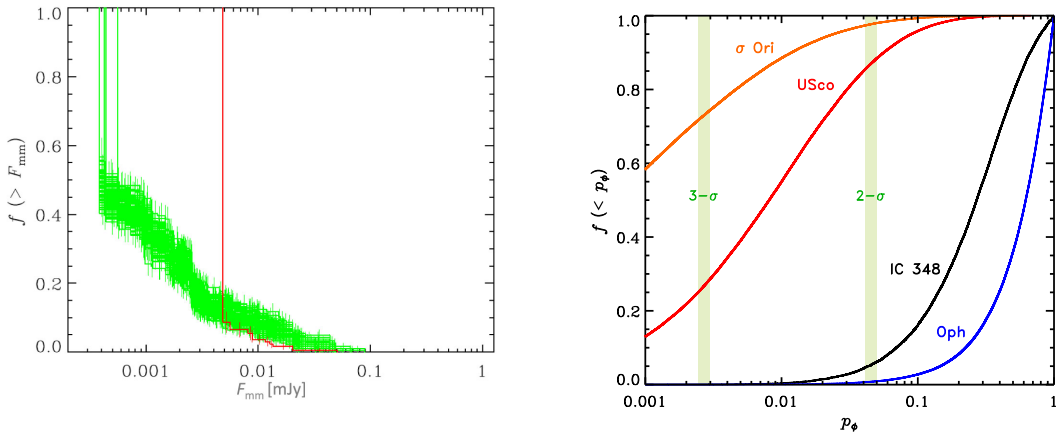

Figure 9. Left: the cumulative distribution function (CDF) of the disc luminosities in IC 348 (red) compared to 100 random draws of the same CDF for Taurus with the same spectral type distribution as in IC 348 (green). The Taurus distribution has been scaled down to compensate for its closer distance (140 versus 320 pc). The fluxes in IC 348 tend to be slightly lower than in Taurus, but this difference is not significant given the available data. Right: the comparison between the disc luminosity distribution of IC 348 and Taurus. The quantity p_ϕ is the probability that two samples statistically belong to the same population. The cumulative distribution of p_ϕ is calculated for 10^5 Monte Carlo simulations. Our results for the IC 348 disc luminosity show no significant discrepancy with those of Taurus. As a reference, similar comparisons have been made for the millimeter surveys of discs in ρ Ophiuchus and Upper Scorpius from Andrews et al. (2013), and σ-Orionis from Williams et al. (2013).

initial conditions effect (e.g. more massive discs tend to form giant planets that result in transition disc SEDs) and/or a disc evolution effect (the formation of one or more massive planets results in both a transition disc SED and a reduction of the accretion rate, increasing the lifetime of the outer disc). Resolved Atacama Large Millimeter/Submillimeter Array (ALMA) images of cluster members could be used to study the structure of these transition discs in detail and to identified additional objects with large cavities among the population of discs that present normal IR SED (i.e. transition objects with partially depleted cavities). A stacking analysis of the Class II/thick discs that individually remain undetected at 850 μm suggests that their median dust mass is $\lesssim$1 $M_\oplus$, corresponding to $M_D \lesssim 0.3\ M_{JUP}$ if a gas-to-dust-mass ratio of 100 is assumed. The IC 348 cluster represents an ideal target to investigate the distribution of disc masses at the 2–3 Myr age range, but the available data is not deep enough to allow a meaningful comparison to older and younger regions. While the estimated median flux of the discs in the cluster ($\lesssim$1 mJy at 850 μm) is well beyond the sensitivity of our SCUBA-2 study, we note that such sensitivity level (5σ) could be reached in $\sim$1 min of integration time per object with the ALMA. Spectroscopic observations with ALMA would also be able to establish the gas content of the discs to investigate the evolution of the gas-to-dust-mass ratio, while multiwavelength photometry (e.g. at 850 μm and 3 mm) could be used to trace the growth of grains up to cm sizes. Such studies in clusters of different ages will eventually provide a deeper understanding of the planet formation time-scales than the *Spitzer* plots of the IR disc fractions as a function of cluster age that are currently used to constrain the time available for planet formation.

ACKNOWLEDGEMENTS

We thanks the anonymous referee whose comments have helped to improve the paper. LAC was supported by ALMA-CONICYT grant number 31120009 and CONICYT-FONDECYT grant number 1140109. LAC, MS, and SC acknowledge support from the Millennium Science Initiative (Chilean Ministry of Economy), through grant 'Nucleus RC13007'.

REFERENCES

Alexander R., Pascucci I., Andrews S., Armitage P., Cieza L., 2014, in Beuther H., Dullemond C. P., Klessen R. S., Henning T. K., eds, Protostars and Planets VI. Univ. Arizona Press, Tuscan, AZ, p. 475
Allen P. R., Luhman K. L., Myers P. C., Megeath S. T., Allen L. E., Hartmann L., Fazio G. G., 2007, ApJ, 655, 1095
Andrews S. M., Rosenfeld K. A., Kraus A. L., Wilner D. J., 2013, ApJ, 771, 129
Beckwith S. V. W., Sargent A. I., Chini R. S., Guesten R., 1990, AJ, 99, 924
Birnstiel T., Andrews S. M., Ercolano B., 2012, A&A, 544, A79
Brauer F., Dullemond C. P., Henning T., 2008, A&A, 480, 859
Calvet N., D'Alessio P., Hartmann L., Wilner D., Walsh A., Sitko M., 2002, ApJ, 568, 1008
Carpenter J. M., Mamajek E. E., Hillenbrand L. A., Meyer M. R., 2006, ApJ, 651, L49
Chapin E. L., Berry D. S., Gibb A. G., Jenness T., Scott D., Tilanus R. P. J., Economou F., Holland W. S., 2013, MNRAS, 430, 2545
Cieza L., Baliber N., 2006, ApJ, 649, 862
Cieza L. et al., 2007, ApJ, 667, 308
Cieza L. A., Swift J. J., Mathews G. S., Williams J. P., 2008, ApJ, 686, L115
Cieza L. A. et al., 2010, ApJ, 712, 925
Cieza L. A., Schreiber M. R., Romero G. A., Williams J. P., Rebassa-Mansergas A., Merín B., 2012a, ApJ, 750, 157
Cieza L. A. et al., 2012b, ApJ, 752, 75
Clanton C., Gaudi B. S., 2014, ApJ, 791, 91
Currie T., Sicilia-Aguilar A., 2011, ApJ, 732, 24
Dodds P., Greaves J. S., Scholz A., Hatchell J., Holland W. S., JCMT Gould Belt Survey Team, 2015, MNRAS, 447, 722
Dodson-Robinson S. E., Salyk C., 2011, ApJ, 738, 131
Dullemond C. P., Dominik C., 2005, A&A, 434, 971
Espaillat C. et al., 2012, ApJ, 747, 103
Espaillat C. et al., 2014, in Beuther H., Dullemond C. P., Klessen R. S., Henning T. K., eds, Protostars and Planets VI. Univ. Arizona Press, Tuscan, AZ, p. 497
Evans N. J., II et al., 2009, ApJS, 181, 321
Feigelson E. D., Nelson P. I., 1985, ApJ, 293, 192
Ford E. B., 2014, Proc. Natl. Acad. Sci., 111, 12616
Fressin F. et al., 2013, ApJ, 766, 81
Furlan E. N. et al., 2006, ApJS, 165, 568

Gorti U., Hollenbach D., 2009, ApJ, 690, 1539
Guilloteau S., Dutrey A., Simon M., 1999, A&A, 348, 570
Hartmann L., Megeath S. T., Allen L., Luhman K., Calvet N., D'Alessio P., Franco-Hernandez R., Fazio G., 2005, ApJ, 629, 881
Herbig G. H., 1998, ApJ, 497, 736
Hernández J. et al., 2007a, ApJ, 662, 1067
Hernández J. et al., 2007b, ApJ, 671, 1784
Howard A. W. et al., 2010, ApJ, 721, 1467
Ireland M. J., Kraus A. L., 2008, ApJ, 678, L59
Kenyon S. J., Hartmann L., 1995, ApJS, 101, 117
Kim K. H. et al., 2013, ApJ, 769, 149
Kraus A. L., Ireland M. J., 2012, ApJ, 745, 5
Lada C. J. et al., 2006, AJ, 131, 1574 (L06)
Lee N., Williams J. P., Cieza L. A., 2011, ApJ, 736, 135
Littlefair S. P., Naylor T., Burningham B., Jeffries R. D., 2005, MNRAS 358, 341
Lubow S. H., Seibert M., Artymowicz P., 1999, ApJ, 526, 1001
Luhman K. L., Rieke G. H., Lada C. J., Lada E. A., 1998, ApJ, 508, 347
Luhman K. L., Stauffer J. R., Muench A. A., Rieke G. H., Lada E. A., Bouvier J., Lada C. J., 2003, ApJ, 593, 1093
Luhman K. L., Lada E. A., Muench A. A., Elston R. J., 2005, ApJ, 618, 810
Mathews G. S., Williams J. P., Ménard F., 2012, ApJ, 753, 59
Mordasini C., Alibert Y., Benz W., Klahr H., Henning T., 2012, A&A, 541, A97
Muench A. A., Lada C. J., Luhman K. L., Muzerolle J., Young E., 2007, AJ, 134, 411 (M07)
Najita J. R., Strom S. E., Muzerolle J., 2007, MNRAS, 378, 369
Owen J. E., Clarke C. J., 2012, MNRAS, 426, L96
Owen J. E., Ercolano B., Clarke C. J., 2011, MNRAS, 412, 13
Pott J.-U., Perrin M. D., Furlan E., Ghez A. M., Herbst T. M., Metchev S., 2010, ApJ, 710, 265
Quillen A. C., Blackman E. G., Frank A., Varnière P., 2004, ApJ, 612, L137
Rebull L. M. et al., 2010, ApJS, 186, 259
Weidenschilling S. J., 1977, Ap&SS, 51, 153
Williams J. P., Cieza L. A., 2011, ARA&A, 49, 67
Williams J. P. et al., 2013, MNRAS, 435, 1671
Wright et al., 2010, AJ, 140, 1868
Zhu Z., Nelson R. P., Hartmann L., Espaillat C., Calvet N., 2011, ApJ, 729, 47

This paper has been typeset from a TEX/LATEX file prepared by the author.